The electroreduction of oxygen in aprotic solvents

Azhar, Azrul; Manyepedza, Tshiamo; Oladeji, Abiola; Hendi, Ruba; Rees, Neil

DOI:
10.1016/j.jelechem.2020.113989

Document Version
Peer reviewed version

Citation for published version (Harvard):
Azhar, A, Manyepedza, T, Oladeji, A, Hendi, R & Rees, N 2020, 'The electroreduction of oxygen in aprotic solvents', *Journal of Electroanalytical Chemistry*, vol. 872, 113989.
https://doi.org/10.1016/j.jelechem.2020.113989

The electroreduction of oxygen in aprotic solvents

Azrul I. Azhar, Tshiamo Manyepedza, Abiola V. Oladeji, Ruba Hendi, Neil V Rees*

School of Chemical Engineering, University of Birmingham, Edgbaston, Birmingham B15 2TT, United Kingdom

An article for submission to: Journal of Electroanalytical Chemistry Special Issue

* Corresponding author

Email: n.rees@bham.ac.uk

Abstract

The electrochemical reduction of oxygen in a range of six polar aprotic solvents is investigated via linear sweep voltammetry at platinum, gold, and carbon fibre microelectrodes. Values for the standard heterogeneous electron transfer rate constant (k_0) are reported, and in all cases follow the trend with electrode material of k_0(C) > k_0(Pt) ~ k_0(Au). The variation in k_0 with solvent is discussed in terms of the Debye model and a dependence on the longitudinal dielectric relaxation constant (τ_L) is found of the form $k_0 \propto \tau_L^{-\theta}$. Static solvent effects are accounted for via consideration of both spherical and connected-spheres models of solvation, and it is found that $\theta \approx 0.65$ indicating that the reduction of dioxygen in these solvents is a non-adiabatic outer-sphere electron transfer.

Introduction

The reduction of dioxygen is of widespread interest due to its ubiquity in many physical and energy-related contexts. Here we consider the use of aprotic solvents as a convenient means of studying the initial electron transfer to dioxygen: this has direct application to those applications where oxygen reduction occurs only in the presence of aprotic solvents (e.g. reactive metal-air batteries), as well as providing a considerable simplification to studying the reaction in aqueous systems.

$$O_2 + e^- \rightleftharpoons O_2^{\cdot -} \quad (1)$$

Previous studies have considered the reduction of oxygen in non-aqueous solvents, including the polarographic generation of superoxide reported by Peover and White [1], to the cyclic voltammetry of Vasudevan and Wendt [2] who measured standard heterogeneous rate constants in acetonitrile, dimethylformamide and dimethylsulfoxide and glassy carbon, graphite and platinum electrodes. These studies primarily reported the reversibility of the voltammetric behaviour, the confirmation of the formation of superoxide as a stable species, and the reporting of heterogeneous rate constants. The kinetics for the one electron reduction can be described most easily via the Butler-Volmer model, where the reductive and oxidative electron transfer rate constants are related to the overpotential (E-E_f^0) via the transfer coefficient (α or β respectively) and the standard heterogeneous electrochemical rate constant (k_0) by [3]:

$$k_{red} = k_0 exp\left(\frac{-\alpha F\left\{E - E_f^0\right\}}{k_B T}\right) \quad (2)$$

and $$k_{ox} = k_0 exp\left(\frac{\beta F\left\{E - E_f^0\right\}}{k_B T}\right) \quad (3)$$

where F is Faraday's constant, k_B is Boltzmann's constant and T the absolute temperature.

The reduction of dioxygen in aprotic solvents is usually considered to be outer-sphere in character, regardless of the nature of the solvent or electrode material [4]. Nevertheless, significant variations have been found in the electrochemical rate constant depending on the electrode or the solvent used. In the case of electrode material, it has been found that carbon electrodes tend to yield faster k_0 values than metallic (i.e. Au, Pt, Pd) surfaces for both oxygen reduction [2,5] and more generally for quinones [6] in aprotic solvents.

In considering the variation in heterogeneous rate constant between solvents, the dielectric properties of each solvent are expected to have a strong influence via either static or dynamic

effects. The former primarily affects the Gibbs energy of activation ($\Delta G^{\ddagger}$) through the solvation of reactant and product species, whereas the latter affects the so-called frequency factor (*A*, eqn (4)).

$$k_0 = Aexp\left(\frac{-\Delta G^{\ddagger}}{k_B T}\right) \quad (4)$$

In particular, the dynamic solvent response to changes in charge distribution on the reacting molecule as it moves towards and through the transition state is likely to fundamentally alter the electron transfer rate [7]. This electrostatic-based coupling between solvent and reacting molecule, or 'dielectric friction' effect can be significant, and can lead to variation in rate constant of several orders of magnitude [2,8].

Here we report the voltammetric study of the reduction of oxygen dissolved in six aprotic solvents, namely acetonitrile, propylene carbonate, chloroform, dichloromethane, 1,2-dichloroethane, and 1,1,1-trichloroethane. Each solvent contained supporting electrolyte and diffusion coefficients and saturated oxygen concentrations were determined. The voltammetry was used to extract values for the standard electrochemical rate constant and transfer coefficient for the reduction reaction at carbon fibre, gold and platinum microelectrodes, and hence to interpret any trends in terms of static and dynamic solvent effects based on simple continuum theory.

Experimental

The following chemicals and gases were obtained commercially and used without further purification: tetra-*n*-butylammonium tetrafluoroborate (TBATFB, Fluka, 99%), acetonitrile (99.8%, Sigma Aldrich), propylene carbonate (>99.0%, Sigma Aldrich), chloroform (99%, Sigma Aldrich), dichloromethane (99%, Sigma Aldrich), 1,2-dichloroethane (99%, Sigma Aldrich), 1,1,1-trichloroethane (99%, Sigma Aldrich), oxygen (N5 grade, BOC Gases plc). All solvents were stored over molecular sieves (4Å, Sigma Aldrich) before use.

All solutions were made with sufficient inert electrolyte (0.40 M) to be fully supported [9] and were thoroughly purged with oxygen before experiments commenced and a positive atmosphere of oxygen was maintained throughout all measurements. The oxygen was pre-saturated with the appropriate dried solvent prior to entering the electrochemical cell to minimise evaporation of the reaction solution.

Electrochemical measurements were made using a three-electrode arrangement in a faraday cage, controlled by a PGSTAT128N potentiostat (Metrohm-Autolab BV, Utrecht, NL) under ambient conditions (T = 292 $\pm$ 2 K). A silver wire quasi-reference electrode and a platinum gauze counter electrode were used. The more typical Ag/Ag^+ reference was found to be impractical in this work as trace leakage of Ag^+ into the cell caused interference at the reducing potentials via electrodeposition of Ag. The working electrodes included a macro glassy carbon disk (GC, diameter 3 mm, BASi Inc.), and a selection of microelectrodes: carbon fibre (radius 5.6 µm, BASi Inc), gold (radius 10.6 µm) and platinum (radius 10.5 µm). Both Au and Pt electrode were fabricated in-house and were of microwire-in-glass construction. All microelectrodes were electrochemically calibrated in ferrocene/acetonitrile solutions and radii found to be in agreement with the nominal diameters of their microwires. Electrodes were thoroughly polished with decreasing sizes of alumina slurries from 9 µm to 0.05 µm on soft lapping pads (Buehler Inc, USA) to a mirror finish.

Results & Discussion

First, linear sweep voltammetry was carried out at (a voltage scan rate of 25 mV s^{-1}) to find the diffusion coefficients and saturated concentrations of dioxygen in the six different solvents using a carbon fibre ultramicroelectrode and a GC macro disk electrode. The measured steady-state limiting current and peak current (I_{Lim} and I_P) respectively from these scans were compared to determine the diffusion coefficient, D, according to the following equations for a 1 electron transfer [3]:

$$I_P = (2.69 \times 10^5)\pi r_d^2 C_{bulk}(Dv)^{1/2} \quad (5)$$

$$I_{Lim} = 4FC_{bulk}Dr_{ume} \quad (6)$$

$$\frac{I_{Lim}}{I_P} = 0.370\left(\frac{r_{ume}}{r_d^2}\right)\left(\frac{D}{v}\right)^{1/2} \quad (7)$$

where F is the Faraday constant, r_d is the radius of the macrodisk electrode, r_{ume} is the radius of the microdisk electrode, α is the transfer coefficient, C_{bulk} is the bulk concentration of the electroactive species (here dioxygen), and v the voltage scan rate. In these cases, the appearance of the voltammetry indicated that the kinetics were in the quasi-reversible range, and so both the irreversible and reversible Randles-Sevčík equations were used to generate values for D and $[O_2]_{sat}$ for comparison with literature. It was found that the reversible Randles-Sevčík derived results gave closest agreement, and so equations (5)-(7) were used throughout (see Supplementary Information). Table 1 gives the resulting values, which are in good agreement with available literature, for example D(ACN + 0.1 M ^{n}Bu$_4$ClO$_4$) = 7.05 $\pm$ 0.53 cm^2 s^{-1} [2], $[O_2]_{sat}$(ACN + 0.1 M ^{n}Bu$_4$ClO$_4$) = 7.43 $\pm$ 0.65 mM [10].

Solvent (containing 0.4 M ^{n}Bu$_4$BF$_4$)	D / × 10^{-5} cm^2 s^{-1}	$[O_2]_{sat}$ / mM
Acetonitrile (ACN)	6.20 $\pm$ 0.20	7.24 $\pm$ 0.19
Propylene carbonate (PC)	3.39 $\pm$ 0.12	1.78 $\pm$ 0.03
Chloroform (CF)	8.09 $\pm$ 0.31	3.42 $\pm$ 0.13
Dichloromethane (DCM)	3.95 $\pm$ 0.15	5.52 $\pm$ 0.35
1,2-Dichloroethane (DCE)	4.00 $\pm$ 0.18	5.62 $\pm$ 0.40
1,1,1-Trichloroethane (TCE)	4.13 $\pm$ 0.20	8.13 $\pm$ 0.14

Table 1. Diffusion coefficients and saturated oxygen concentrations determined at 292 $\pm$ 2 K

Next, a series of linear sweep voltammograms were recorded for each microelectrode (Pt, C, Au) in an oxygen-saturated solution of 0.4 M TBATFB in acetonitrile. The voltammograms were analysed in a two-step process: first, estimated values of the standard heterogeneous rate constant (k_0) and transfer coefficient (α) were obtained via the Mirkin and Bard method of quartile potentials [11], and secondly, these were refined by manual waveshape fitting using DigiElch software (www.elchsoft.com) using the Butler-Volmer formalism due to the known difficulties in fitting quasi-reversible and irreversible voltammetry using the symmetric Marcus-Hush formalism [12-14]. A minimum of five voltammograms were analysed in this way for each microelectrode, and the whole process repeated for each solvent. The results are summarised in table 2, with typical 'best-fit' plots illustrated in figure 1 (see Supplementary Information for more). The derived values for the formal

potentials (E_f^0) vary considerably, which we ascribe to the use of a quasi-reference electrode (see the Supplementary Information).

		Solvent (with 0.4 M TBATFB added)					
		ACN	**PC**	**CF**	**DCM**	**DCE**	**TCE**
Au	k_0 / 10^{-3} cm s^{-1}	10.0 ± 0.3	2.3 ± 0.2	1.3 ± 0.2	2.5 ± 0.1	3.7 ± 0.3	1.5 ± 0.1
	α (all ± 0.01)	0.28	0.36	0.33	0.30	0.34	0.32
C	k_0 / 10^{-3} cm s^{-1}	43.0 ± 4.0	8.9 ± 0.1	1.3 ± 0.3	10.0 ± 0.9	11.0 ± 0.1	9.0 ± 0.3
	α (all ± 0.01)	0.42	0.41	0.32	0.38	0.40	0.28
Pt	k_0 / 10^{-3} cm s^{-1}	9.3 ± 0.1	1.6 ± 0.2	1.0 ± 0.1	2.7 ± 0.4	5.0 ± 0.3	0.8 ± 0.1
	α (all ± 0.01)	0.27	0.34	0.33	0.32	0.35	0.29

Table 2. Summary of data fitting results for the kinetic parameters of oxygen reduction reaction.

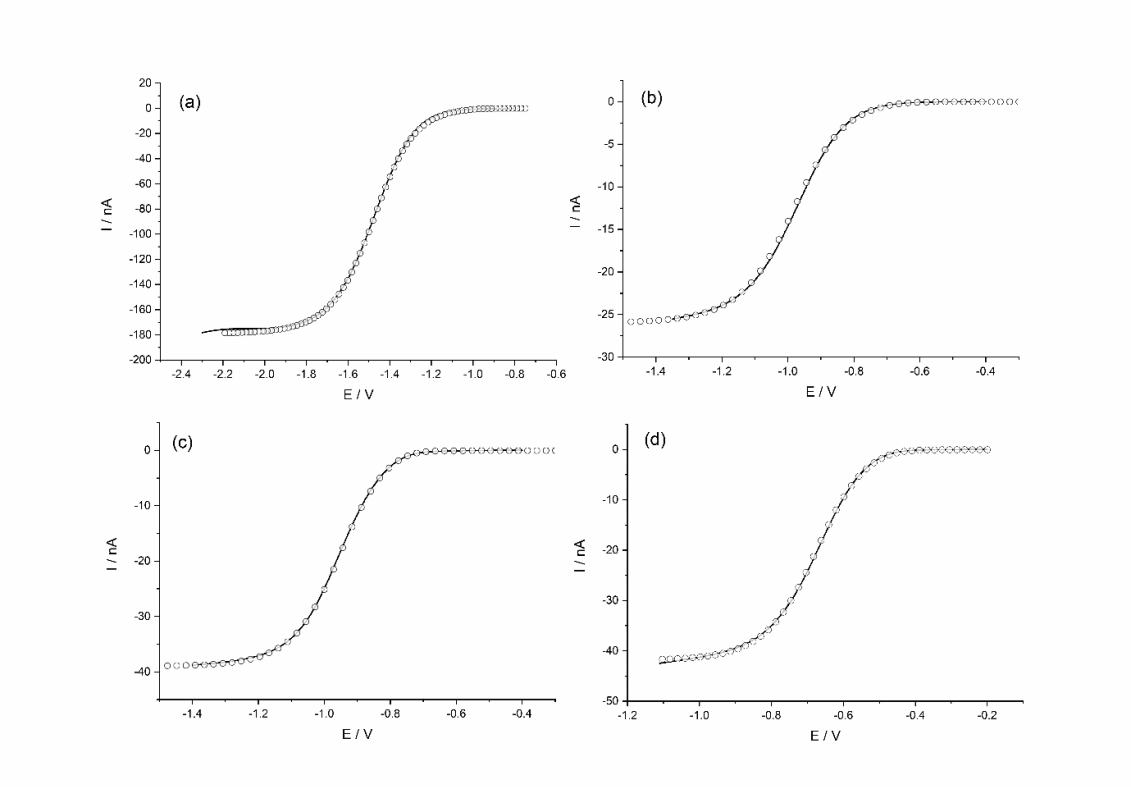

Figure 1: Illustrative simulation vs experiment fits for oxygen reduction in solutions of 0.4 M TBATFB for the following combinations of electrode/solvent: (a) Pt/ACN, (b) Pt/PC, (c) C/DCM, and (d) C/DCE.

Since any discussion of the effects of electrode materials may be affected by double layer effects due to the chosen concentration of supporting electrolyte, additional experiments were conducted at concentrations of TBATFB of 0.25 and 0.60 M. These concentrations were chosen to ensure that they were a minimum of 30 times higher than that of the oxygen reduction reaction was fully supported. No significant difference in the derived rate constant or transfer coefficient was observed (see Supporting Information).

The results show that the rate constants for oxygen reduction at Au and Pt electrodes are of a similar rate, and considerably lower than at the carbon fibre electrode. This is in agreement with previous

studies which reported the same trend for the reduction of quinones in acetonitrile [6] and of oxygen in dimethylsulfoxide [5], albeit in contradiction with Levich-Dogonadze-Kuznetsov (LDK) theory which predicted that the rate constant on a Pt surface should be 3 orders of magnitude greater than that at carbon due to the difference in electronic density at the Fermi levels. [15,16]. In the cases above [5,6], the acceleration due to the carbon surface was ascribed to the significantly greater effectiveness (estimated as 11-fold) of *sp*-band states compared to *d* band states in coupling [5,17] as well as any specific solvent-electrode adsorption effects that will alter the plane of closest approach of reactants and hence the attenuation coefficient.

In comparing the absolute values of rate constants and transfer coefficients with available literature, the latter are in general agreement in being generally low and in the range 0.25-0.35 [18,19]. One discrepancy is the k_0 at Pt in ACN, which has been reported to be approx. 0.02 cm s^{-1} [18] albeit for a solution of 0.05 M tetrabutylammonium hexafluorophosphate.

The solvent effect on the electron transfer rates has been considered by several groups, particularly in determining the dynamic component. [7,20-26] The simplest treatments of the solvent continuum model, where the reacting solute molecule is treated as a point charge/dipole in a spherical cavity formed within a continuum (i.e. structureless) solvent continuum, predicts an inverse relationship between k_0 and the longitudinal dielectric relaxation time in the adiabatic limit.

The general expression from Marcus for the standard electrochemical rate constant is:

$$k_0 = \kappa v_n exp\left(\frac{-\Delta G^{\ddagger}}{k_B T}\right) \tag{8}$$

where κ is the electronic transmission constant, and v_n is the nuclear barrier-crossing frequency [27]. The value of κ varies from 1 in the adiabatic limit, to smaller values as the degree of non-adiabaticity increases. This will be influenced by the inner-sphere activation barrier and the interaction between Gibbs energy surfaces of reactant and product (via the electronic matrix coupling factor). The nuclear barrier-crossing frequency is determined by the vibrational modes within the reactant and solvent, and depends on the relative magnitudes of the inner and outer-sphere contributions (v_{is} and v_{os}) to the activation barrier. A convenient representation, that utilises the relationship between the outer-sphere contribution and the solvent longitudinal relaxation time (τ_L), is [27]

$$v_n = v_{is}^{1-\theta} \tau_L^{-\theta} \tag{9}$$

and so in general

$$\ln k_0 = -\theta ln\tau_L + \ln\left\{\kappa v_{is}^{1-\theta} exp\left(\frac{-\Delta G^{\ddagger}}{k_B T}\right)\right\} \tag{10}$$

where τ_L is the longitudinal dielectric relaxation constant, and θ and is a constant. In the adiabatic limit, reactant and product states couple strongly and the electron transfer reaction can be considered in terms of the motion of the nuclei on a single potential energy surface – in the case of outer-sphere reactions the nuclear motion is the same as the solvent and so electron transfer rates are directly proportional to solvation rates, and so predict θ = 1. In the non-adiabatic limit, however, where reactant and product states are very weakly coupled, such that the probability for electron transfer is very low and rate limiting, solvent dynamics do not affect the overall rate and so θ = 0 is expected. Various experimental reports have provided values of θ ranging from 0.2 to 1 [28,29], and this variation can be due to several effects. For example, the solvent may not behave as a structureless continuum where molecules in the solvent respond to changes in charge distribution

via rotational reorientation (i.e. a 'Debye solvent'), or the degree of curvature of the activation energy barrier top may lead to different solvent effects on barrier crossing and deactivation [30].

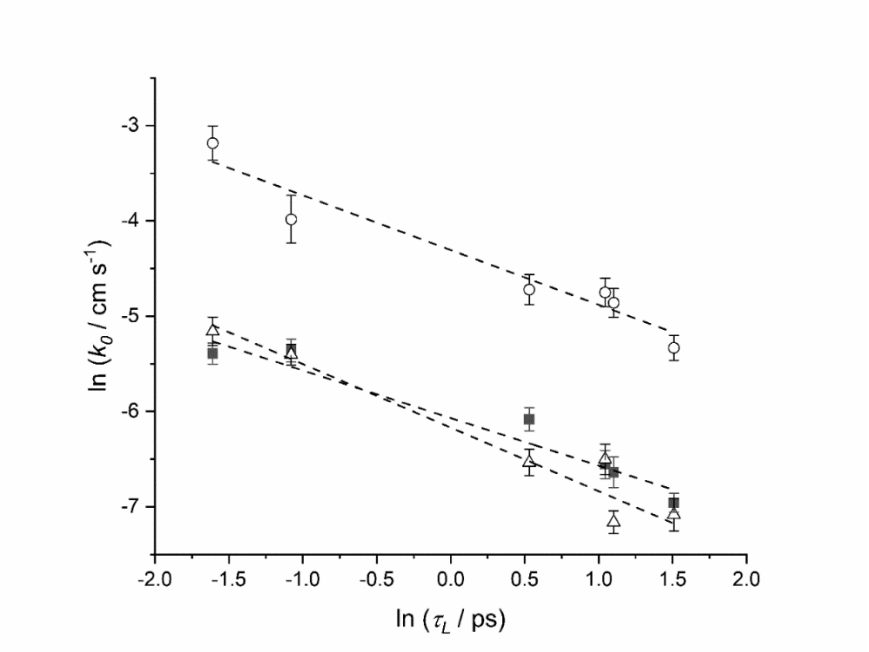

Figure 2. Logarithmic plot of k_0 vs. τ_L for oxygen reduction in the six solvents measured at Au (■), C (○), and Pt (△) electrodes. Each dataset is fitted with a least-squares best fit line.

Figure 2 shows a logarithmic plot of the derived values of k_0 against the reported longitudinal dielectric relaxation times for the six solvents under consideration (ACN 0.20 ps [31], PC 1.70 ps [32], CF 3.1 ps [33], DCM 0.34 ps [34], DCE 2.84 ps [35], and TCE 4.52 ps [35]). Data was not available for the 0.4 M TBATFB – solvent solutions, and so the plot utilises data for pure solvents only. The gradients of the best-fit lines give fairly similar values of θ for the oxygen reduction at Au (θ = 0.50, R^2 = 0.935), C (θ = 0.57, R^2 = 0.927), and Pt (θ = 0.64, R^2 = 0.948). This plot reflects both static and dynamic solvent effects, however, since the solvent-specific effects on the Gibbs energy of activation have not been accounted for. It has been shown that by removing the static effects can be informative as to the relative magnitudes of the static and dynamic effects [36]. As a first approximation, this can be done by assuming the Born solvation energy to be equivalent of the outer-sphere component of the reorganisation energy (λ_o). This modifies eqn (11) to be (see Supplementary Information)

$$\ln k_0 + \left(\frac{e^2}{32k_BT\pi\varepsilon_0}\frac{\gamma}{\varepsilon_r}F(a,d)\right) = -\theta ln\tau_L + B \qquad (12)$$

where $= ln\left(\kappa v_{is}^{1-\theta}\right) + \frac{\lambda_{is}}{4k_BT}$, and *F(a,d)* is a function of *a* (the molecular or atomic radius) and *d* the distance of closest approach to the electrode (i.e. the plane of electron transfer). The exact form of *F(a,d)* depends on whether a simple spherical or connected-spheres model is used for the reactant molecule (see the Supporting Information for further details). Here the non-spherical models due to Peover & Powell [37], Hale [38], and Fawcett & Kharkats [39] are used for simplicity: whilst not truly ellipsoidal, all three models treat the reactant molecule as two connected spheres, which in the present case would appear most appropriate. The relevant forms here are:

Spherical Born model: $$F(a,d) = \frac{1}{a} - \frac{1}{2d} \quad (13)$$

where *a* is the molecular (spherical) radius and *d* the distance of closest approach.

Connected spheres models:

(1) Peover & Powell $$F(a,d) = \frac{\delta_1^2}{a} + \frac{\delta_2^2}{b} - \frac{1}{2d} \quad (14)$$

(2) Hale $$F(a,d) = \frac{\delta_1^2}{a} + \frac{\delta_2^2}{b} - \frac{2\delta_1\delta_2}{r_{ab}} \quad (15)$$

(3) Fawcett & Kharkats

$$F(a,d) = \frac{\delta_1^2}{a} + \frac{\delta_2^2}{b} - \frac{2\delta_1\delta_2}{r_{ab}} - \delta_1^2 f(r_{ab},b) - \delta_2^2 f(r_{ab},a) - \frac{\delta_1^2}{d_1} - \frac{\delta_2^2}{d_2} - \frac{2\delta_1\delta_2}{d} \quad (16)$$

and $$f(r_i,r_j) = \frac{r_i}{2\left(r_i^2 - r_j^2\right)}\left\{\frac{r_j}{r_i} - \left(1 - \left(\frac{r_j}{r_i}\right)^2\right) ln\left(\frac{r_i + r_j}{\left[r_i^2 - r_j^2\right]^{1/2}}\right)\right\}$$

In the above three models, the radii of the connected spheres are *a* and *b*, the distance between the centres of the spheres is r_{ab}, and *d* is the distance of closest approach. The spheres are taken to carry fractional charges, δ_1 and δ_2. To evaluate the most appropriate model to apply in this study, all experimental results have been analysed under each model in figure 3 (see Supporting Information

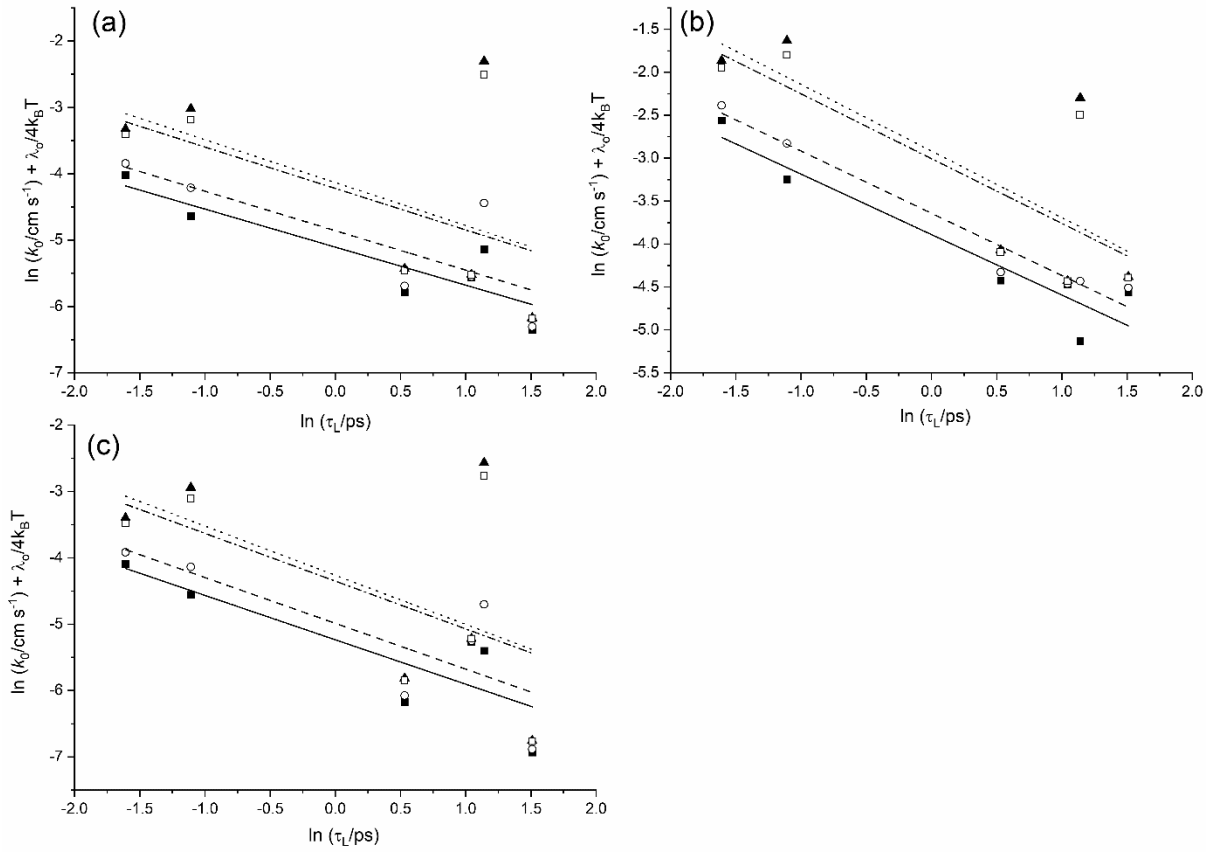

Figure 3. Comparison of the above four models using experimental data for (a) gold, (b) carbon, and (c) platinum microelectrodes in each of the solvents. In each case the data points and best-fit lines

respectively are denoted by: for the spherical model (■, —), Peover and Powell (○,---), Hale (▲,⋯), and Fawcett and Kharkats (□, -·-).

It was found that of the four models, the spherical Born model yielded the highest R^2 values across the three data sets, indicating the best fit to the data. We postulate therefore that this model is the most appropriate for application to our data, and suggest that the physical basis of this may due to a lack of a preferred orientation of the oxygen molecule in which to undergo electron transfer. Given the symmetry of the LUMO π^* orbital this suggests that there is no strong preference of and end-on or face-on approach of the O_2 molecule *vis á vis* orbital overlap with electronic states on the electrode.

A plot of equation 12 & 13 is shown in figure 4, with gradients in close agreement for all three materials of Au (θ = 0.57, R^2 = 0.787), C (θ = 0.70, R^2 = 0.902), and Pt (θ = 0.67, R^2 = 0.698). This confirms that the observed values of θ are due to both static and dynamic solvent effect and that the oxygen reduction is non-adiabatic.

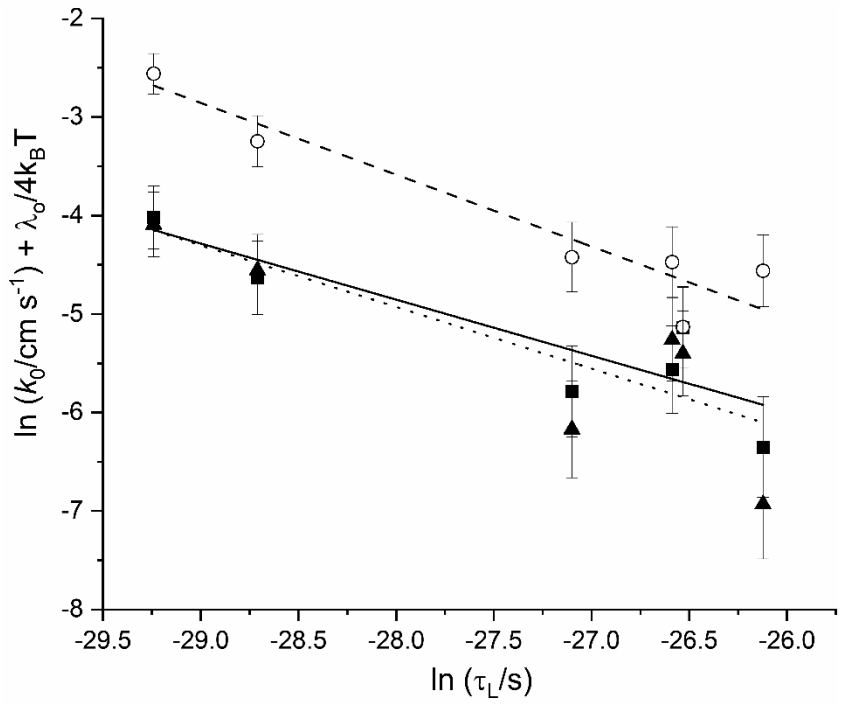

Figure 4. Plot of k_0 (adjusted for λ_o) vs. τ_L (now in s) for oxygen reduction in the six solvents measured at Au (■), C (○), and Pt (△) electrodes. Each dataset is fitted with a least-squares best fit line.

The intercepts of these best fit lines are found to be within error of each other, specifically: -20.8 ± 3.6 (Au), -24.0 ± 2.6 (C), and -22.4 ± 5.0 (Pt). This is consistent with the format of equation 12, where the intercept was given as $B = ln\left(\kappa v_{is}^{1-\theta}\right) + \frac{\lambda_{is}}{4k_BT}$, since none of these terms are expected to be influenced by electrode material in the case of an outer-sphere electron transfer.

Conclusions

The reduction of oxygen at Au, Pt and carbon fibre microelectrodes has been studied in the solvents: acetonitrile, propylene carbonate, chloroform, dichloromethane, dicholoroethane, and

trichloroethane. Diffusion coefficients and saturated oxygen concentrations have been reported, several of which are for the first time. The electron transfer kinetics have been determined, with k_0 and α values given, and shown to be non-adiabatic and outer-sphere in character in the six aprotic solvents studied and for the three electrode materials, using simple continuum solvent models. Apparent effects due to static solvent effects have been adjusted for.

Acknowledgements

The authors thank the EPSRC (grant no. EP/G037116/1) for funding.

Appendix A. Supplementary data

Supplementary data to this article can be found at ….

References

1. M.E. Peover, B.S. White, Electrochim. Acta 11 (1966) 1061

2. D. Vasudevan, H. Wendt, J. Electroanal. Chem. 192 (1995) 69

3. A.J. Bard, L.R. Faulkner, Electrochemical Methods: Fundamentals and Applications, 2nd Ed., Wiley, New York, 2001.

4. C. Hartnig, M. Koper, J. Electroanal. Chem. 532 (2002) 165

5. R. Hendi, P.H. Robbs, B. Sampson, R. Pearce, N.V. Rees, J. Electroanal. Chem. 829 (2018) 16

6. R. Nissim, C. Batchelor-McAuley, R.G. Compton, Chem. Commun. 48 (2012) 3294

7. M. Maroncelli, J. MacInnis, G.R. Fleming, Science 243 (1989) 1674

8. M. Opallo, J. Chem. Soc. Faraday Trans. 1, 82 (1986) 339

9. E.J.F. Dickinson, J.G. Limon-Petersen, N.V. Rees, R.G. Compton, J. Phys. Chem. C 113 (2009) 11157

10. N.V. Rees, D.Phil. Thesis, University of Oxford. 2004.

11. M.V. Mirkin, A.J. Bard, Anal. Chem. 64 (1992) 2293

12. M.C. Henstridge, E. Laborda, N.V. Rees, R.G. Compton, Electrochim. Acta 84 (2012) 12

13. D. Suwatchara, N.V. Rees, M.C. Henstridge, E. Laborda, R.G. Compton, J. Electroanal. Chem. 665 (2012) 38

14. D. Suwatchara, M.C. Henstridge, N.V. Rees, R.G. Compton, J. Phys. Chem. C 115 (2011) 14876

15. M. Opallo, B. Behr, A. Kapturkiewicz, J. Electroanal. Chem. 182 (1985) 427

16. R.R. Dogonadze, in ‘Reactions of Molecules at Electrodes’, N.S. Hush (Ed.), Wiley, London. 1971

17. S. Gosavi, R.A. Marcus, J. Phys. Chem. B 104 (2000) 2067

18. P.S. Jain, S. Lal, Electrochim. Acta 27 (1982) 759

19. R.G. Evans, O.V. Klymenko, S.A. Saddoughi, C. Hardacre, R.G. Compton, J. Phys. Chem. B 108 (2004) 7878

20. E.W. Castner Jr, B. Bagchi, M. Maroncelli, S.P.Webb, A.J. Ruggiero, G.R Fleming, Ber. Bunsenges. Phys. Chem. 92 (1988) 363

21. I. Rips, J. Jortner, J. Chem. Phys. 87 (1987) 2090

22. I. Rips, J. Jortner, Chem. Phys. Lett. 133 (1987) 411

23. M. Sparpaglione, S. Mukamel, J. Phys. Chem. 91 (1987) 3938

24. H. Sumi, R.A. Marcus, J. Chem. Phys. 84 (1986) 4894

25. L.D. Zusman, Chem. Phys. 49 (1980) 295

26. H. Heitele, Angew. Chem. Int. Ed. 32 (1993) 359

27. W.R. Fawcett, M. Opallo, Angew. Chem. Int. Ed. 33 (1994) 2131

28. H. Fernandez, M.A. Zon, J. Electroanal. Chem. 332 (1992) 237

29. W.R. Fawcett, C.A. Foss Jr, J. Electroanal. Chem. 270 (1989) 103

30. J.T. Hynes, J. Phys. Chem. 90 (1986) 3701

31. K. Mansingh, A. Mansingh, J. Chem. Phys. 41 (1964) 827

32. M.A. Kahlow, T.J. Kang, P.F. Barbara, J. Chem. Phys. 88 (1988) 2372

33. J. Goulon, J.L. Rivali, J.W. Fleming, J. Chamberlain, G.W. Chantry, Chem. Phys. Lett. 18 (1973) 211

34. C.J. Reid, Spectrochim. Acta 38A (1982) 697

35. J. Crossley, S. Walker, J. Chem. Phys. 45 (1966) 4733

36. M.J. Weaver, T. Gennett, Chem. Phys. Lett. 113 (1985) 213

37. M.E. Peover, J.S. Powell, J. Electroanal. Chem. 20 (1969) 427

38. J.M. Hale, in ‘Reactions of Molecules at Electrodes’, N.S. Hush (Ed.), Wiley, London. 1971.

39. W.R. Fawcett, Yu. I. Kharkats, J. Electroanal. Chem. 47 (1973) 413

The electroreduction of oxygen in aprotic solvents

Azrul Azhar, Tshiamo Manyepedza, Abiola V. Oladeji, Ruba Hendi, Neil V Rees*

School of Chemical Engineering, University of Birmingham, Edgbaston, Birmingham B15 2TT, United Kingdom

Supplementary Information

Section 1: Determination of diffusion coefficients and saturated oxygen concentrations

	ACN	PC	CF	DCM	DCE	TCE
I_{peak} / A (GC macro)	1.72×10^{-4}	7.65×10^{-5}	1.83×10^{-4}	2.61×10^{-4}	2.69×10^{-4}	1.58×10^{-4}
I_{Lim} / A (C micro)	9.25×10^{-8}	1.27×10^{-8}	6.00×10^{-8}	3.82×10^{-8}	4.10×10^{-8}	6.35×10^{-8}
I_{Lim} / I_{peak}	5.38×10^{-4}	1.66×10^{-4}	3.28×10^{-4}	1.46×10^{-4}	1.52×10^{-4}	4.02×10^{-4}
Based on Reversible Randles-Sevcik Eqn:						
D / cm^2 s^{-1}	6.20×10^{-5}	3.39×10^{-5}	8.09×10^{-5}	3.95×10^{-5}	4.00×10^{-5}	4.13×10^{-5}
$[O_2]_{sat}$ / mM	7.24	1.78	3.42	5.52	5.62	8.13
Based on Irreversible Randles-Sevcik Eqn:						
α	0.42					
D / cm^2 s^{-1}	2.11×10^{-5}	6.20×10^{-5}	6.20×10^{-5}	6.20×10^{-5}	6.20×10^{-5}	6.20×10^{-5}
$[O_2]_{sat}$ / mM	183.0					
Literature values for comparison:						
D / cm^2 s^{-1}	7.05 ± 0.53					
$[O_2]_{sat}$ / mM	8.1					
Reference	[1]					

Given the implausible values obtained using the irreversibile Randles-Sevcik equation, the reversible form was used throughout to determine diffusion coefficients and saturated concentrations.

Section 2: Best-fit plots of simulation and experiment

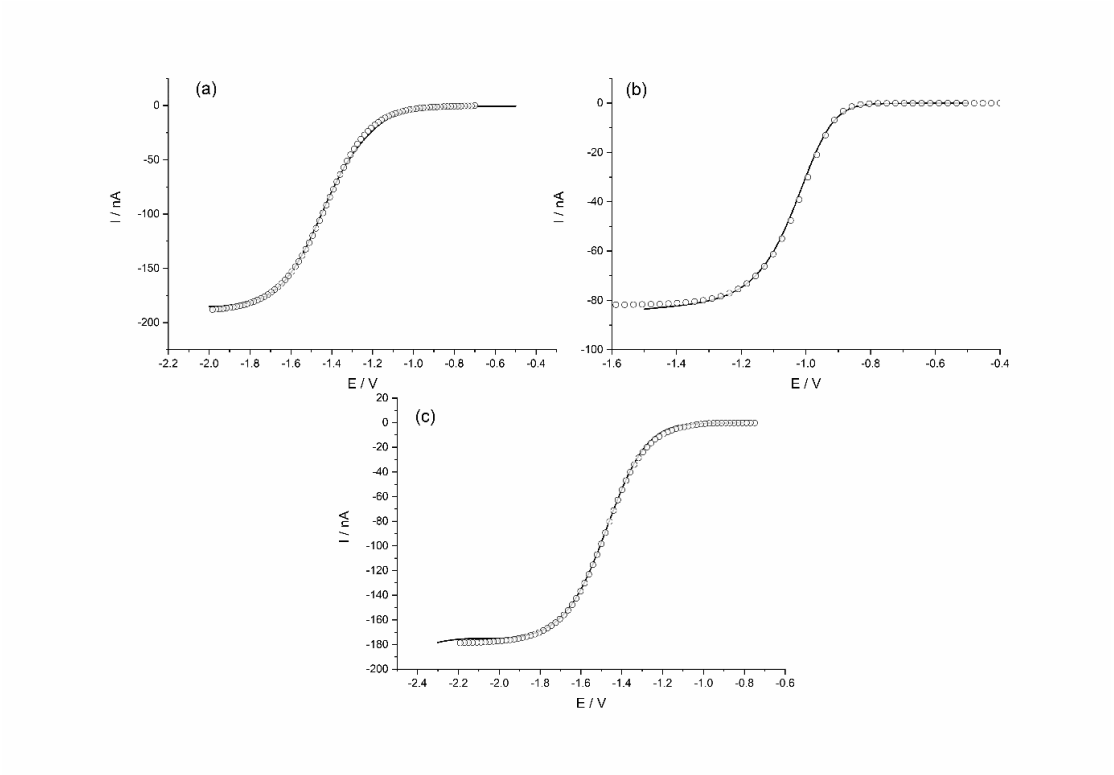

Figure S1. Plots of experimental data (—) and best-fit simulation (○) for the oxygen reduction reaction at (a) Au, (b) carbon fibre, and (c) Pt microelectrodes in 0.4 M tetrabutylammonium tetrafluoroborate in acetonitrile.

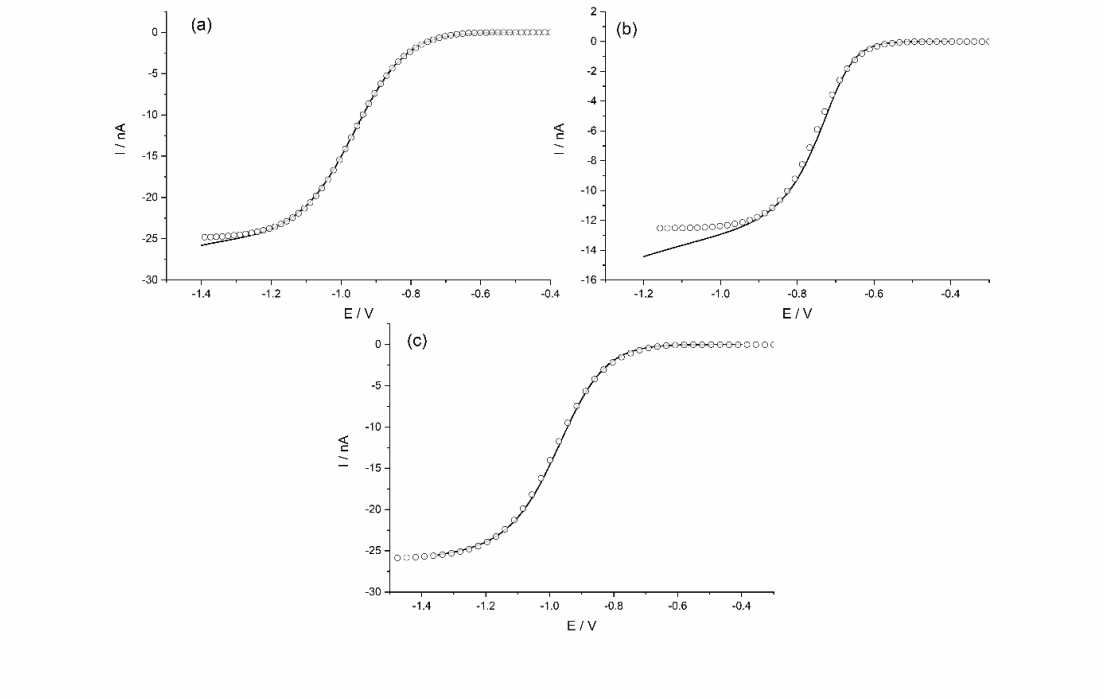

Figure S2. Plots of experimental data (—) and best-fit simulation (○) for the oxygen reduction reaction at (a) Au, (b) carbon fibre, and (c) Pt microelectrodes in 0.4 M tetrabutylammonium tetrafluoroborate in propylene carbonate.

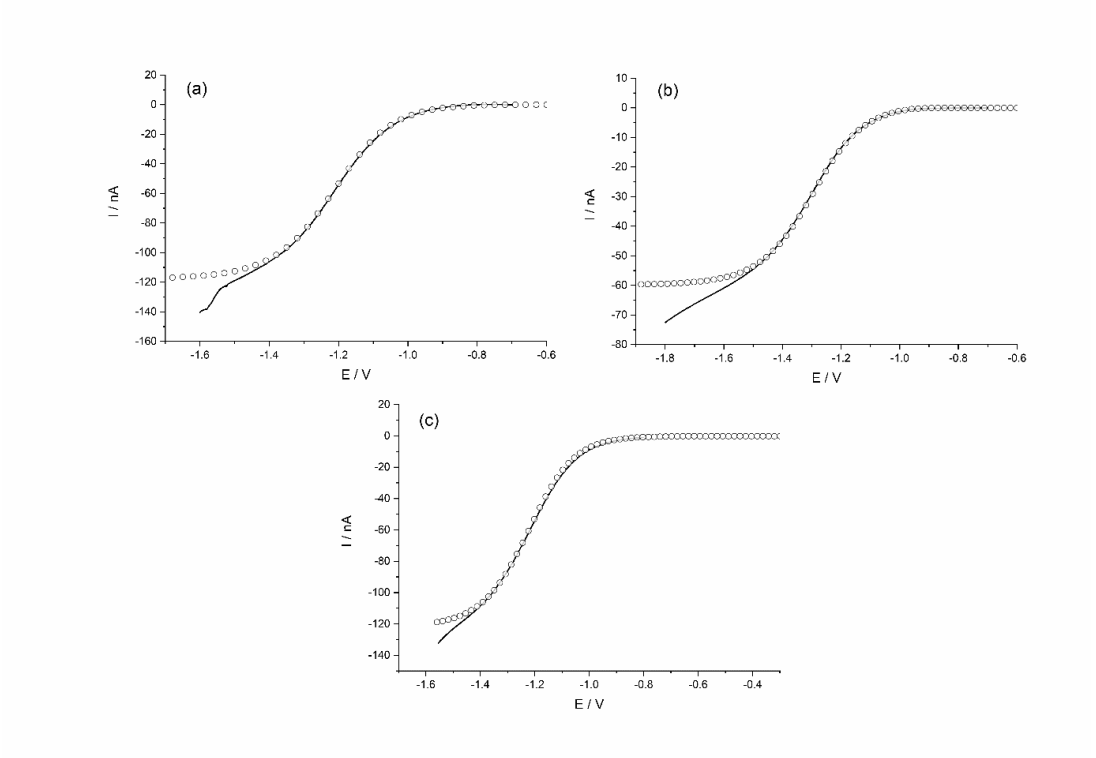

Figure S3. Plots of experimental data (—) and best-fit simulation (○) for the oxygen reduction reaction at (a) Au, (b) carbon fibre, and (c) Pt microelectrodes in 0.4 M tetrabutylammonium tetrafluoroborate in chloroform.

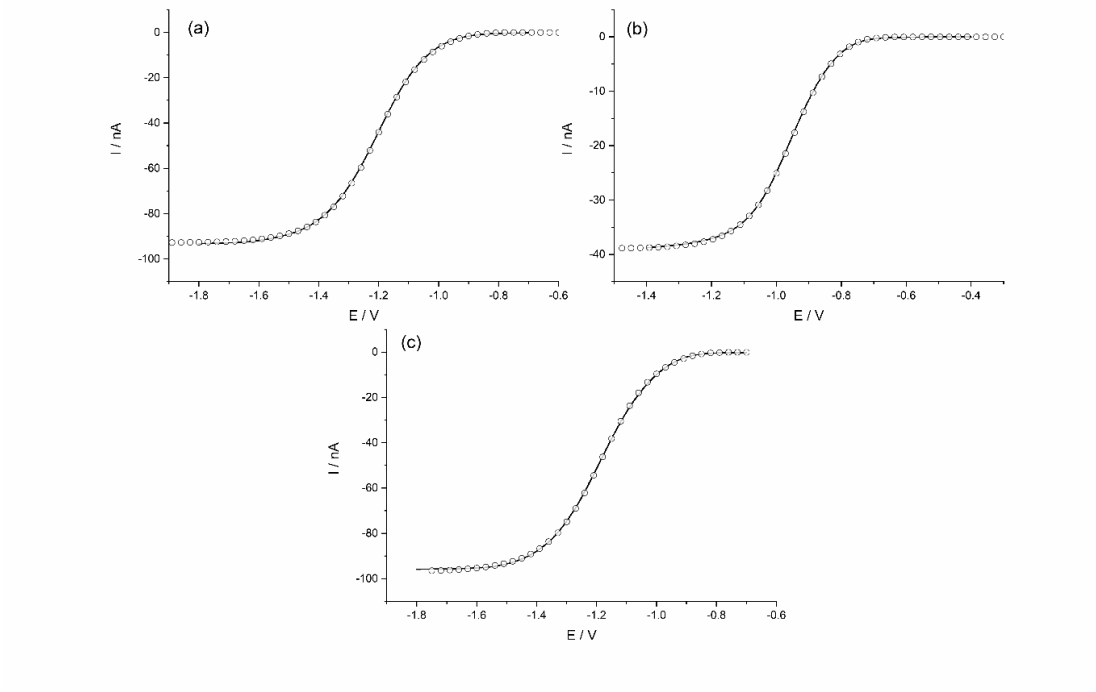

Figure S4. Plots of experimental data (—) and best-fit simulation (○) for the oxygen reduction reaction at (a) Au, (b) carbon fibre, and (c) Pt microelectrodes in 0.4 M tetrabutylammonium tetrafluoroborate in dichloromethane.

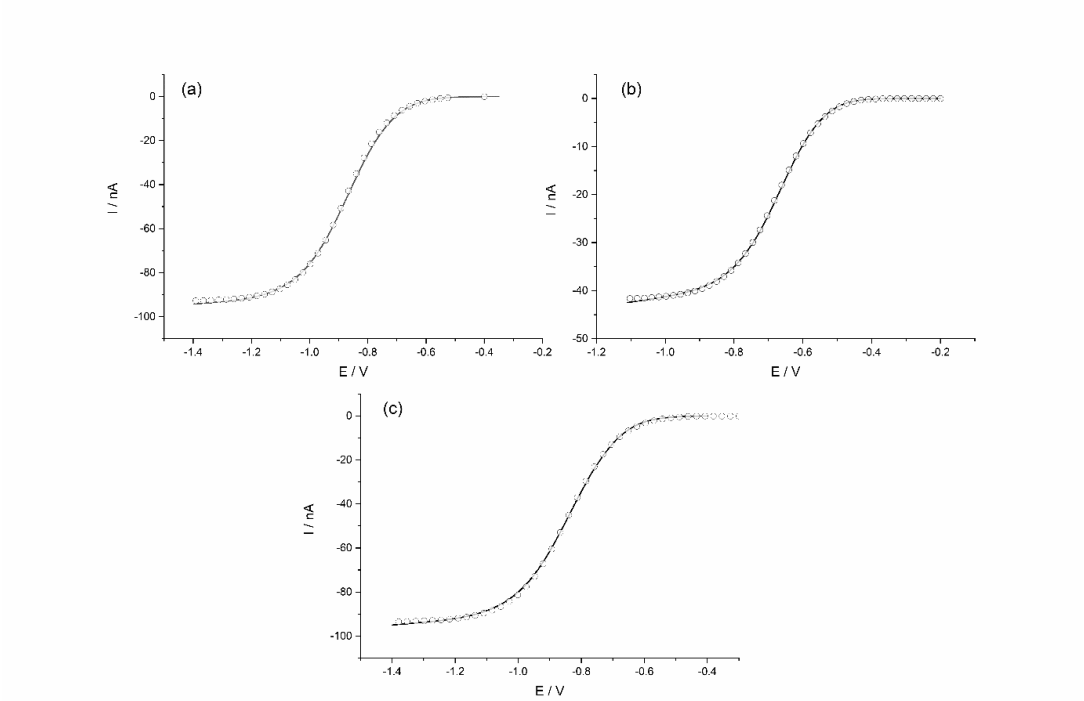

Figure S5. Plots of experimental data (—) and best-fit simulation (○) for the oxygen reduction reaction at (a) Au, (b) carbon fibre, and (c) Pt microelectrodes in 0.4 M tetrabutylammonium tetrafluoroborate in 1,2-dichloroethane.

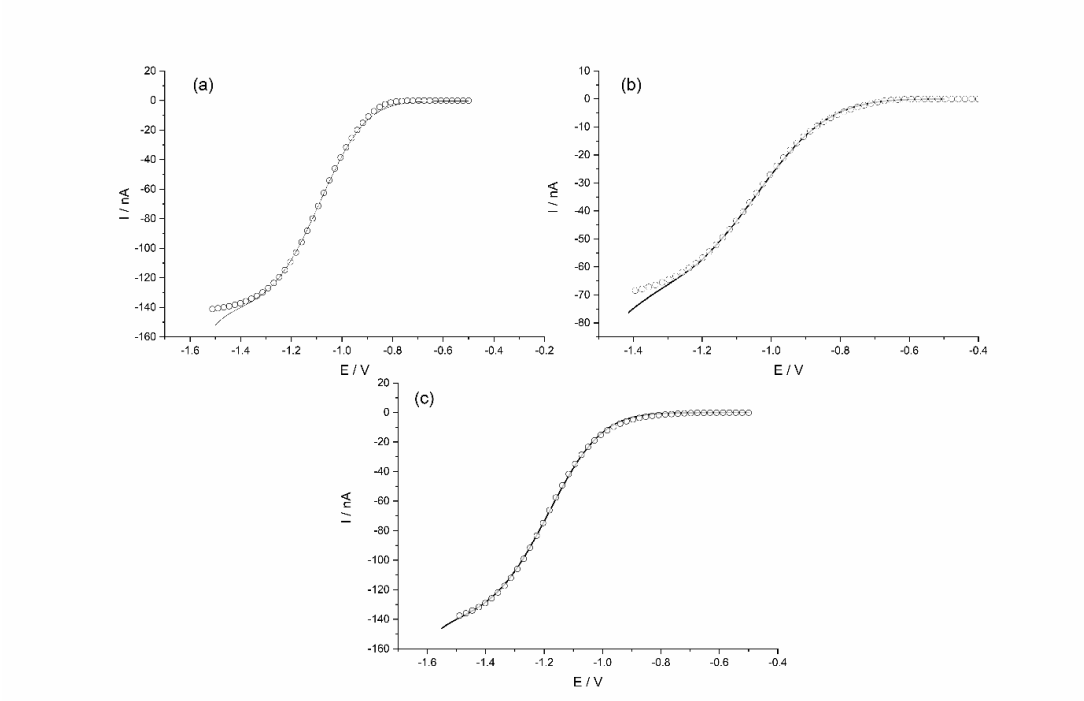

Figure S6. Plots of experimental data (—) and best-fit simulation (○) for the oxygen reduction reaction at (a) Au, (b) carbon fibre, and (c) Pt microelectrodes in 0.4 M tetrabutylammonium tetrafluoroborate in 1,1,1-trichloroethane.

Section 3: Effect of varying concentration of supporting electrolyte

		[NBu_4BF_4] / mol dm^{-3}		
		0.25	**0.40**	**0.60**
Au	k_0 / 10^{-3} cm s^{-1}	2.5 ± 0.1	2.5 ± 0.2	2.7 ± 0.2
	α (all ± 0.01)	0.31	0.30	0.32
C	k_0 / 10^{-3} cm s^{-1}	11.3 ± 0.6	10.0 ± 0.9	11.5 ± 1.3
	α (all ± 0.01)	0.36	0.38	0.38
Pt	k_0 / 10^{-3} cm s^{-1}	3.2 ± 0.3	2.7 ± 0.4	3.2 ± 0.3
	α (all ± 0.01)	0.31	0.32	0.34

The concentration of supporting electrolyte was varied to investigate if there was a significant double layer effect. Dichloromethane was selected as a test system for this study. The concentrations were selected to be a minimum of 30 times higher than that of the oxygen concentration to ensure full support. The values suggest that there is no systematic effect for this case.

Section 4: Approximate separation of static and dynamic solvent effects and evaluation of solvent models

The general expression from Marcus for the standard electrochemical rate constant is:

$$k_0 = Aexp\left(\frac{-\Delta G^{\ddagger}}{k_B T}\right) \quad \text{(S1)}$$

Where the pre-exponential factor can be expressed as

$$A = \kappa v_n \quad \text{(S2)}$$

Here κ is the electronic transmission constant, and v_n is the nuclear barrier-crossing frequency [2]. The value of κ varies from 1 in the adiabatic limit, to smaller values as the degree of non-adiabaticity increases. This will be influenced by the inner-sphere activation barrier and the interaction between Gibbs energy surfaces of reactant and product (via the electronic matrix coupling factor).

The nuclear barrier-crossing frequency is determined by the vibrational modes within the reactant and solvent, and depends on the relative magnitudes of the inner and outer-sphere contributions (v_{is} and v_{os}) to the activation barrier. A convenient representation, that utilises the relationship between the outer-sphere contribution and the solvent longitudinal relaxation time (τ_L), is [2]

$$v_n = v_{is}^{1-\theta}\tau_L^{-\theta} \quad \text{(S3)}$$

In the adiabatic limit θ=1, but is often less than unity where either the inner sphere activation energy barrier is significant or where there is some dree of non-adiabaticity [2].

The approximation is often made for the Gibbs energy of activation that:

$$\Delta G^{\ddagger} \approx \frac{1}{4}(\lambda_o + \lambda_i) \quad \text{(S4)}$$

Here the terms λ_o and λ_i refer to the outer-sphere and inner-sphere reorganisation energy respectively. The former is often in turn approximated to the Born solvation energy:

$$\lambda_o = \frac{e^2\gamma}{8\pi\varepsilon_0\varepsilon_r}F(a,d) \tag{S5}$$

where *e* is the electronic charge, ε_0 and ε_r are the permittivity of free space and relative permittivity of the medium respectively, and *F(a,d)* is a function of *a* (the molecular or atomic radius) and *d* the distance of closest approach to the electrode (i.e. the plane of electron transfer). The exact form of *F(a,d)* is discussed below. γ is the Pekar factor for the solvent.

Combining (S1) to (S3), we can write

$$k_0 = Aexp\left(\frac{-\lambda_o}{4k_BT}\right)exp\left(\frac{-\lambda_i}{4k_BT}\right) \tag{S6}$$

$$k_0 = \kappa\nu_n exp\left(\frac{-e^2}{32k_BT\pi\varepsilon_0}\frac{\gamma}{\varepsilon_r}F(a,d)\right)exp\left(\frac{-\lambda_i}{4k_BT}\right) \tag{S7}$$

$$k_0 exp\left(\frac{e^2}{32k_BT\pi\varepsilon_0}\frac{\gamma}{\varepsilon_r}F(a,d)\right) = \kappa\nu_{is}^{1-\theta}\tau_L^{-\theta}exp\left(\frac{-\lambda_i}{4k_BT}\right)$$

Taking logarithms we get

$$\ln k_0 + \left(\frac{e^2}{32k_BT\pi\varepsilon_0}\frac{\gamma}{\varepsilon_r}F(a,d)\right) = \ln\left(\kappa\nu_{is}^{1-\theta}\tau_L^{-\theta}\right) - \left(\frac{\lambda_i}{4k_BT}\right) \tag{S8}$$

Since the pre-exponential term contains several sub-terms, including the $\tau_L^{-\theta}$ term, we arrive at an expression in the form of eqn (11) in the main text

$$\ln k_0 + \left(\frac{e^2}{32k_BT\pi\varepsilon_0}\frac{\gamma}{\varepsilon_r}F(a,d)\right) = -\theta ln\tau_L + \ln B \tag{S9}$$

where $B = ln\left(\kappa\nu_{is}^{1-\theta}\right) + \frac{\lambda_{is}}{4k_BT}$

In the absence of specific solvent-electrode adsorption, the factor $\frac{\gamma}{\varepsilon_r}$ is the only one that varies with solvent.

Next we turn to the form of the function *F(a,d).* The most commonly used form is assuming the reactant is spherical. However, this is clearly not applicable in general, and variants have been proposed to reflect ellipsoidal geometries, usually by treating the reactant molecule as two (or more) spheres. This would appear to be most appropriate in this case, for a diatomic oxygen molecule. The relevant forms here are:

Spherical Born model: $$F(a,d) = \frac{1}{a} - \frac{1}{2d} \tag{S10}$$

where *a* is the molecular (spherical) radius and *d* the distance of closest approach.

Connected spheres models:

(1) Peover & Powell $$F(a,d) = \frac{\delta_1^2}{a} + \frac{\delta_2^2}{b} - \frac{1}{2d} \tag{S11}$$

(2) Hale $$F(a,d) = \frac{\delta_1^2}{a} + \frac{\delta_2^2}{b} - \frac{2\delta_1\delta_2}{r_{ab}} \tag{S12}$$

(3) Fawcett & Kharkats

$$F(a,d) = \frac{\delta_1^2}{a} + \frac{\delta_2^2}{b} - \frac{2\delta_1\delta_2}{r_{ab}} - \delta_1^2 f(r_{ab},b) - \delta_2^2 f(r_{ab},a) - \frac{\delta_1^2}{d_1} - \frac{\delta_2^2}{d_2} - \frac{2\delta_1\delta_2}{d} \qquad \text{(S13)}$$

And $$f(r_i,r_j) = \frac{r_i}{2\left(r_i^2 - r_j^2\right)}\left\{\frac{r_j}{r_i} - \left(1 - \left(\frac{r_j}{r_i}\right)^2\right) ln\left(\frac{r_i + r_j}{\left[r_i^2 - r_j^2\right]^{1/2}}\right)\right\}$$

In the above three models, the radii of the connected spheres are *a* and *b*, the distance between the centres of the spheres is r_{ab}, and *d* is the distance of closest approach. The spheres are taken to carry fractional charges, δ_1 and δ_2.

To evaluate the most appropriate model to apply in this study, we have analysed all experimental results under each model. For use in eqns S10-S13 we have taken the values of the molecular radius of oxygen to be 152 pm, the atomic radius to be 60.4 pm and the O-O bond length to be 121 pm [3]. The distance of closest approach has been set to the diameter of the particular solvent molecule to assume an outer-sphere mechanism; larger values of ca. 10 Å can also be adopted.[4,5]. The fractional charges (δ_1 and δ_2) have been set to be 0.5 each. The values of the permittivity and Pekar factors for the solvents in questions are given below:

Solvent	$\boldsymbol{\varepsilon_r}$	$\boldsymbol{\gamma}$	**Ref.**
ACN	36.6	0.53	6
PC	64.9	0.48	7,8
CF	4.81	0.27	9
DCM	8.93	0.30	10
DCE	10.36	0.0095	11
TCE	7.53	0.028	11

The following figures compare the four models given by equations S10-S13, and the table summarises the results.

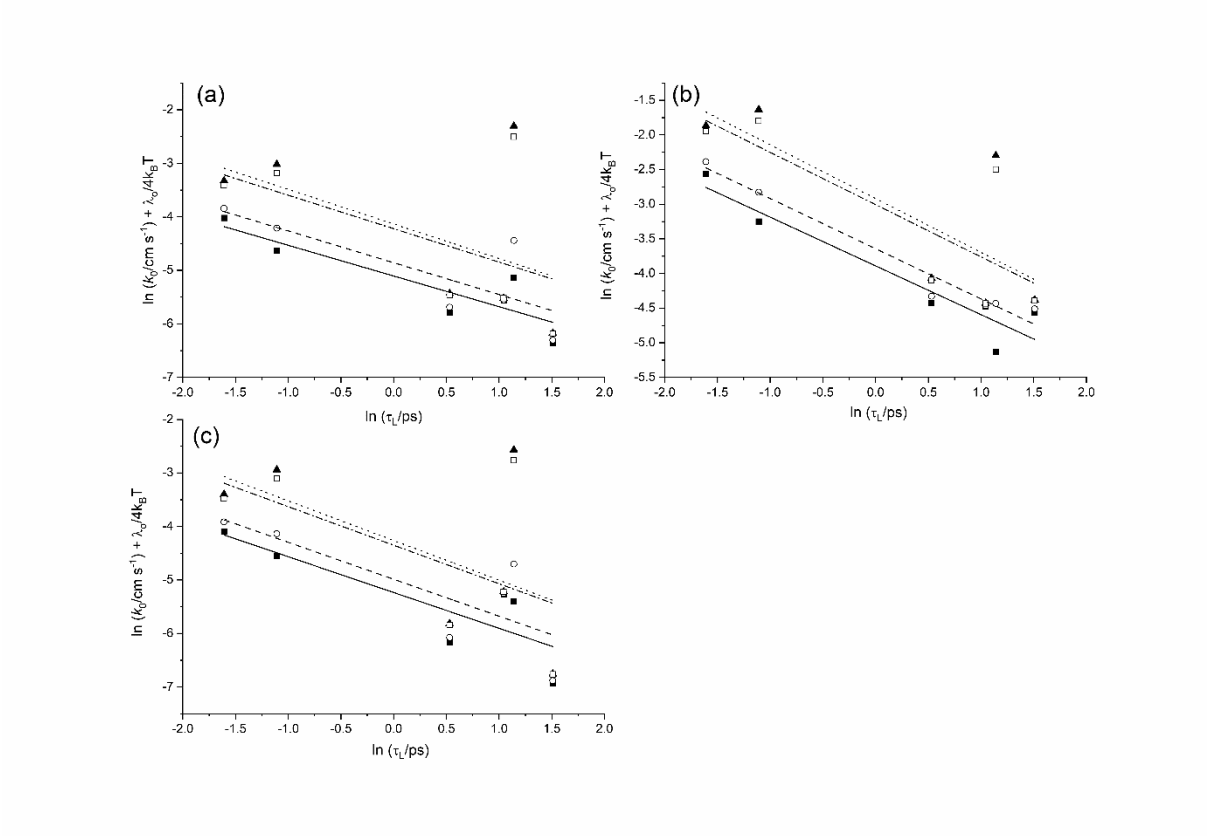

Figure S7. Comparison of the above four models using experimental data for (a) gold, (b) carbon, and (c) platinum microelectrodes. In each case the data points and best-fit lines respectively are denoted by: for the spherical model (■, —), Peover and Powell (○,---), Hale (▲,⋯), and Fawcett and Kharkats (□, -·-).

Model	**Au**		**C**		**Pt**	
	Gradient	**R^2**	**Gradient**	**R^2**	**Gradient**	**R^2**
Spherical	-0.574	0.787	-0.704	0.902	-0.670	0.698
Peover & Powell	-0.595	0.625	-0.725	0.966	-0.690	0.604
Hale	-0.646	0.272	-0.776	0.538	-0.741	0.314
Fawcett & Kharkats	-0.625	0.282	-0.755	0.616	-0.720	0.324

It is found that the of the four models, the spherical Born model produces the highest R^2 values across the three data sets, indicating the best fit to the data. We postulate therefore that this model is the most appropriate for application to our data, and suggest that the physical basis of this may due to a lack of a preferred orientation of the oxygen molecule in which to undergo electron transfer. Given the symmetry of the LUMO π^* orbital this suggests that there is no strong preference

of and end-on or face-on approach of the O_2 molecule *vis á vis* orbital overlap with electronic states on the electrode.

References

[1] D. Vasudevan, H. Wendt, J. Electroanal. Chem. 192 (1995) 69, quoted in 0.1 M Et_4NClO_4.

[2] W.R. Fawcett, M. Opallo, Angew. Chem. Int. Ed. 33 (1994) 2131

[3] CRC Handbook of Chemistry and Physics, D.R. Lide (Ed), 84th Edition, CRC Press, Boca Raton, USA. 2003.

[4] J.M. Hale, in 'Reactions of Molecules at Electrodes', N.S. Hush (Ed.), Wiley, London. 1971.

[5] C.E. Banks, R.G. Compton, Understanding Voltammetry, 3rd Edn., World Scientific Press, Singapore. 2018.

[6] K. Mansingh, A. Mansingh, J. Chem. Phys. 41 (1964) 827

[7] M.A. Kahlow, T.J. Kang, P.F. Barbara, J. Chem. Phys. 88 (1988) 2372

[8] B.Y. Mladenova, D.R. Kattnig, B. Sudy, P. Choto, G. Grampp, PCCP 18 (2016) 14442

[9] J. Goulon, J.L. Rivali, J.W. Fleming, J. Chamberlain, G.W. Chantry, Chem. Phys. Lett. 18 (1973) 211

[10] C.J. Reid, Spectrochim. Acta 38A (1982) 697

[11] J. Crossley, S. Walker, J. Chem. Phys. 45 (1966) 4733